Check for updates

Manufacturing of poly(ethylene glycol diacrylate)-based hollow microvessels using microfluidics†

Saurabh S. Aykar,[a] David E. Reynolds,[a] Marilyn C. McNamara[a] and Nicole N. Hashemi 🆔 *[ab]

The microvasculature is a vital organ that distributes nutrients within tissues, and collects waste products from them, and which defines the environmental conditions in both normal and disease situations. Here, a microfluidic chip was developed for the fabrication of poly(ethylene glycol diacrylate) (PEGDA)-based hollow self-standing microvessels having inner dimensions ranging from 15 μm to 73 μm and displaying biocompatibility/cytocompatibility. Macromer solutions were hydrodynamically focused into a single microchannel to form a concentric flow regime, and were subsequently solidified through photopolymerization. This approach uniquely allowed the fabrication of hollow microvessels having a defined structure and integrity suitable for cell culturing.

1. Introduction

The human microvasculature network forms the interface between organ parenchyma and circulating blood and is located within the tissue of operating organs such as brain, liver, kidneys, *etc.*[1] More specifically, the human microvasculature system is a branched web consisting of tubularly structured arterioles (10–100 μm diameter in size), capillaries (4–12 μm diameter in size), and venules (10–100 μm diameter in size).[1–5] Together, these microvessels control the microcirculation of nutrients, oxygen supply, and waste between tissues and blood in the human body.[2–14] However, due to the complex and variable physiological processes that these microvessels partake in during invasive and noninvasive states, there is a lack of knowledge on how the human microvasculature system naturally functions.[6] An array of *in vivo* and *ex vivo* studies have been conducted to uncover the extensive physiological behaviors of the microvasculature in homeostasis, disease, and medically prevalent conditions. *In vivo* subjects for the testing and study of microvessels in medical and disease-related environments have included mice,[15,16] rats,[17–20] cats,[20,21] and hamsters.[22,23] Unfortunately, these non-human animals lack some of the cellular and tissue interactions found in the human microvasculature systems. Besides *in vivo* systems, *ex vivo* models have been used to some extent for studying human microvessels under various conditions.[24,25] Under these *ex vivo* conditions, however, the preservation of real whole human blood and tissue

can restrict the output of experimental results, and biases can arise during donor selection.[25–27] Fortunately, by recreating human microvessels *in vitro*, these *in vivo* and *ex vivo* barriers can be overcome. For instance, microfluidic devices have been found to enable the precision control of dynamic-flow environments, endothelial cell culture, and physiological properties of an *in vitro* 3D microvasculature system for days on end.[26–35] Examples of tissue-engineered microvessels can be found in the human lung,[36,37] heart,[38] kidneys[39] and blood–brain barrier,[40] and have been used to treat sickle-cell and thrombotic diseases.[41,42] In our microfluidic device, though, we have set out to exclude the manual rolling of films and complex cell-seeding procedures and produce a simple platform for generating hollow synthetic multiaxial microvessels. This process includes deploying a combination of chevrons, polymer-based solutions, and a photopolymerization reaction to generate freestanding microvessels.

Our methodology for recreating hollow microvessels *in vitro* takes advantage of the ability of using our coaxial microvessel fabrication technique to construct biocompatible freestanding microvessels. This technique involves the 3D modeling and milling of two distinct microchips. Both chips include a discrete pattern of chevrons in order to produce constant and controlled fluid flow rates. To physically constrain both chips, the direct bonding of poly(methyl methacrylate) (PMMA) is applied using the solvent-assisted thermal bonding technique. After successful fabrication of the model, hollow microtubes are formed through the constant perfusion and overlaying of poly(ethylene glycol diacrylate) (PEGDA) and polyethylene glycol (PEG) solutions in the microchannels of the model. PEGDA forms a hydrophilic covalently crosslinked polymer. The cytocompatibility and biomaterial properties of PEGDA enable it to be photopolymerized into a hydrogel that

[a]Department of Mechanical Engineering, Iowa State University, Ames, IA 50011, USA. E-mail: nastaran@iastate.edu

[b]Department of Biomedical Sciences, Iowa State University, Ames, IA 50011, USA

† Electronic supplementary information (ESI) available. See DOI: 10.1039/c9ra10264g

is resistant to protein absorption, and that can be lithographically modeled and spatially controlled, proving useful for tissue and bioengineering.[43–46] Other research groups, including Uwamori et al.[40] and Daniele et al.,[47] have used fibrin gel and poly(ethylene glycol) dimethacrylate (PEGDMA) for the polymer-based foundations of their microvessels. However, based on the literature,[44–46] PEDGA may behave more suitably as the tissue foundation for our synthetic microvessels, due to the molecular toughness and defined permeability of the polymer.[44–46] After the overlaying of core (PEG), cladding (PEDGA), and sheath (PEG) solutions, a photopolymerization reaction is applied to produce solid, hollow microvessels. The viability of utilizing a photopolymerization reaction with microfluidics to solidify polymer-based materials and mixtures has been investigated extensively by other groups.[48–53] Moreover, unlike the other standard microvessel devices,[36–42] our multiaxial microvessel system has been optimized by testing a variety of chevron dimensions under various flow rates.

In the current work, we constructed two coaxial microfluidic devices with various chevron geometries and examined the effects of these alterations on the surfaces and diameters of the hollow microvessels. Our first microfluidic device was constrained by the dimensions 0.375 mm (width) × 0.250 mm (depth). The dimensions of our second microvessel device were larger, at 0.381 mm × 0.381 mm (width × depth). Ultimately, this design created more stable microvessels that contained a tubular structure with uniform wall barriers and surface finish on the inner and outer surface. Most importantly, though, the microvessels produced from the second chip contained grooves on the outer surface. In this instance, cells could be conveniently cultured along these grooves, assisting in the conversion of the synthesized materials to biological microvessels. Hence, since no previous research has explored these effects, we believe that these findings will provide insight into the applicability and potential of using appropriate size chevrons to develop synthetic microtubes that closely resemble human microvessels. However, to further maximize the ability to use the microvessel chip for the purpose of producing biocompatible freestanding microvessels, we investigated the optimal flow rate ratio (FRR), specifically to reduce microvessel diameters. Through this testing, we discovered that the ideal core : cladding : sheath FRR for the first and second chips were 85 : 20 : 120 µL min^{-1} and 80 : 20 : 120 µL min^{-1}, respectively. We hope that the discoveries of this study will contribute to the ability to use microfluidic devices to create synthetic microvessels for the purpose of replicating and studying the human vasculature system in vitro.

2. Results and discussion

Fig. 1 shows a schematic diagram of a microfluidic device designed to fabricate hollow microvessel fibers. It was designed to contain a microchannel with three inlet channels converging onto the core channel, with the core channel having two shaping regions located on either side of the third inlet channel, and with each shaping region comprised of four chevron-shaped grooves extending vertically on either side of the core channel. An aqueous mixture of non-polymer fluid and poly(ethylene glycol) (PEG) was made to flow through the inlets of the core and sheath solutions whereas an aqueous mixture of pre-polymer fluid and poly(ethylene glycol) diacrylate (PEGDA) was made to flow through the inlet of the cladding solution. The insoluble cladding fluid was made to merge with the core fluid and compress it to form a laminar flow regime having the former one flowing along the side walls of the microchannel and the latter flowing in between. This process of forcing the fluids to converge and pass through a small channel is called hydrodynamic focusing. This partially developed flow regime was then made to flow through the shaping region where the cladding fluid engulfed the core fluid by wrapping the top and bottom domains of the flow regime. Subsequently, the sheath fluid was made to enter through the last inlet and to separate the cladding fluid, laterally, from the walls, and after passing through the last set of chevrons, the sheath fluid was made to engulf the flow from all sides. The flow regime became fully developed after it passed through the last set of chevrons, at which point it was ready to undergo the photopolymerization process. The microfluidic chip was entirely covered with aluminum foil to prevent any pre-solidification of pre-polymer solution in the chevrons or microchannel. A beam of ultraviolet (UV) light was focused on the fully developed flow regime, just below the tip of the microfluidic device, to initiate a photopolymerization reaction, which solidified the cladding fluid while the core and sheath solutions remained unaffected. The UV light beam was focused continuously for 20 s to generate a long hollow microfiber. The microfibers exiting the microfluidic device were allowed to flow in the DI water bath and were
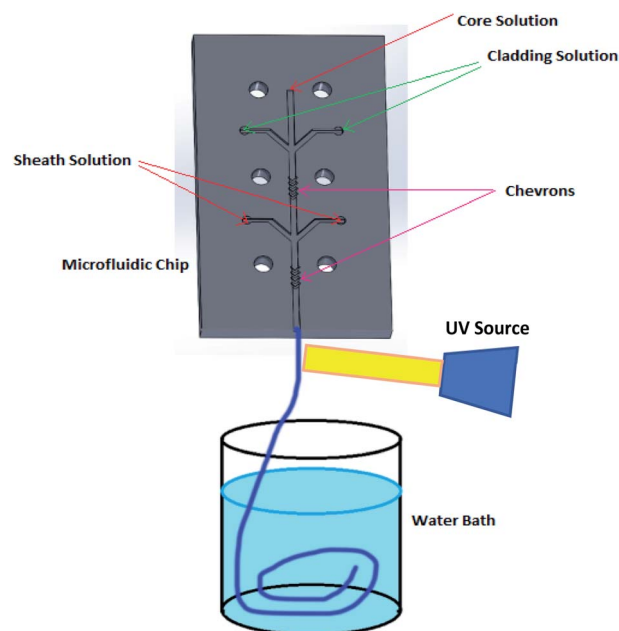

Fig. 1 Schematic diagram illustrating the process used to fabricate hollow microvessels using a PMMA-based microfluidic device.
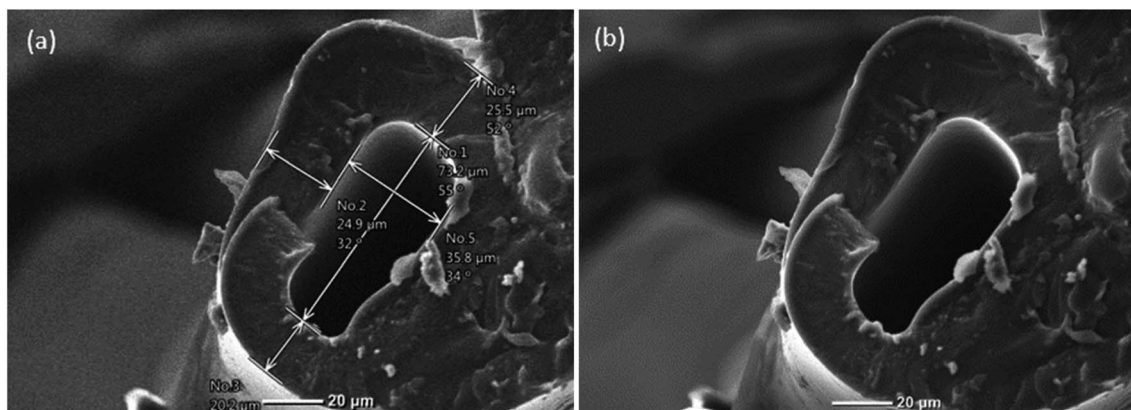
Fig. 2 (a) A scanning electron microscope (SEM) image of a cross section of a hollow PEGDA microvessel fiber depicting the outer wall thickness and inner hole dimension. Scale bar is 20 μm. (b) SEM image of a hollow microvessel fiber generated from a microfluidic device having comparatively smaller chevron dimensions.

then collected using copper wire after the photopolymerization occurred.

The overall size of the hollow microvessels generated depended on the dimensions of the constructed 3D micro-fluidic device. The core channel limited the maximum outer dimensions of the hollow microvessels that could be generated. Moreover, it governed the size of the hollow microvessels in the lateral direction by generating different flow rates of the core, cladding and sheath fluids through their respective inlets. Correspondingly, the dimensions of the chevrons determined the size of the hollow microvessels in the vertical direction. The lateral dimension of the hollow microvessels could be altered dynamically, during the experiment, by changing the flow rates of the core, cladding and sheath fluids. However, the vertical
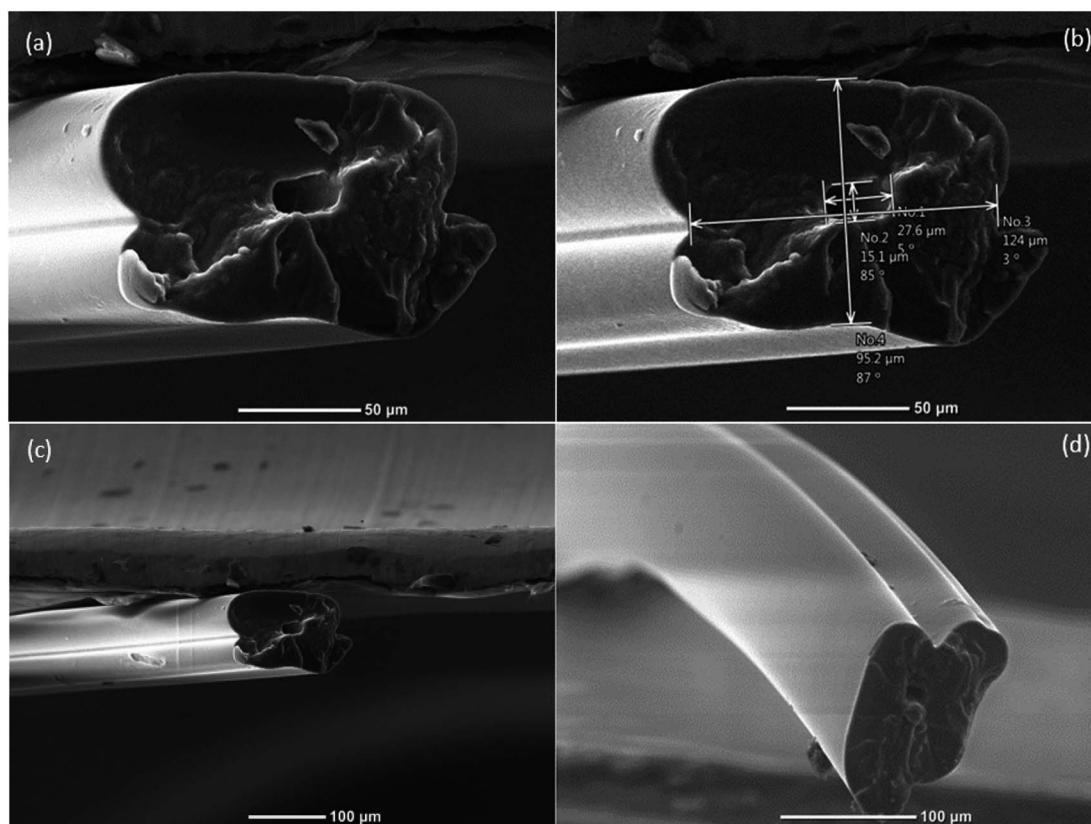

Fig. 3 (a) An SEM image of a cross-section of a hollow microvessel fiber fabricated from a microfluidic device having larger chevron dimensions. (b) Inner and outer dimensions of the hollow microvessel fiber generated. Scale bar is 50 μm. (c) and (d) SEM images of hollow microvessels showing the degree of surface finish and uniformity obtained throughout their length. Scale bar is 100 μm.
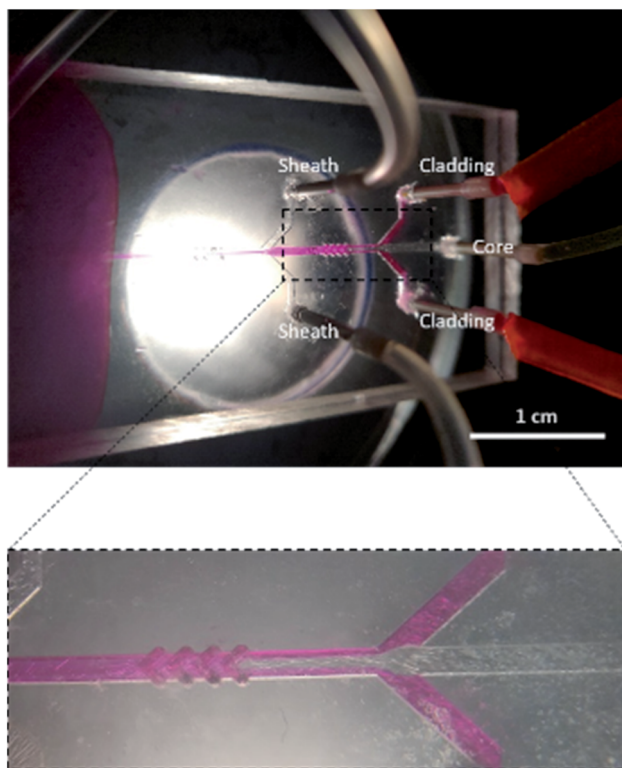
Fig. 4 A microfluidic chip during its operation. The cladding fluid (pink fluid) compresses the core fluid (transparent fluid) without mixing and engulfs it from all sides in the chevrons. Scale bar is 1 cm.

dimension of the microvessel fiber, which depended on the dimensions of the chevrons, could not be altered during the experiment. Hence, there is a need to investigate the effects of different sizes of chevrons on the structure of the hollow microvessel fibers.

The dimensions of the microfluidic channel of the first microfluidic device fabricated were 1.00 mm × 0.750 mm (width × height) and those of the corresponding chevrons were 0.375 mm × 0.250 mm (width × depth). Similarly, the dimensions of the second microfluidic channel were 1.00 mm × 0.750 mm (width × height) and those of the chevrons were 0.381 mm × 0.381 mm (width × depth). Hence, by keeping the dimensions of the core channel the same for both cases, the chevron features were altered. The altered design had, comparatively, more room available for the advection of the flow regime containing PEGDA in the vertical direction, ultimately producing uniformity in the flow regime as seen in Fig. 3. The uniformity was achieved because the fluid could wrap around the vertical domain without any size constraints. According to Poiseuille's law, the greater the size of the chevrons, the lower the resistance offered to the flow by the walls. Initially, we started experimenting with 30 wt% concentrations of both PEGDA and PEG in DI water. However, we noticed that the microfibers obtained with this concentration were either not hollow or showed uneven hollowness throughout their length, and were not stable. The concentration of each of the solutions was then gradually increased from 30 wt% to 50 wt% and the morphology of the obtained hollow microvessel at a concentration of 50 wt% was observed to be stable and to even have hollow attributes throughout its length. A particular flow rate ratio (FRR) was selected by experimenting with various flow rates and examining their respective results. A core : cladding : sheath FRR of 85 : 20 : 120 μL min^{-1} was selected for the first chip, and the concentrations of PEGDA and PEG used were 50 wt% in DI water mixed with 4 wt% of Irgacure and 50 wt% in DI water, respectively. Fig. 2 shows the hollow microvessels generated from the first chip. Similarly, the core : cladding : sheath FRR used for the second chip was 80 : 20 : 120 μL min^{-1} and the concentrations of the solutions were kept the same. The hollow polymer microvessels fabricated from the latter one were observed to have smaller diameters with higher wall thicknesses, which made them stable. The self-standing attribute of the hollow microvessel generated having inner dimensions as small as 15 μm was novel.

The viscosity of the solutions used equally played a crucial role in the uniformity and surface topology of the microvessels. The viscosities of both aqueous solutions (50 wt% PEGDA and 50 wt% PEG) were measured by using a Canon-Fenske viscometer and multiple readings were taken. The average viscosities of aqueous PEGDA and aqueous PEG were determined to be 8.60 mm^2 s^{-1} and 8.68 mm^2 s^{-1}, respectively. Since
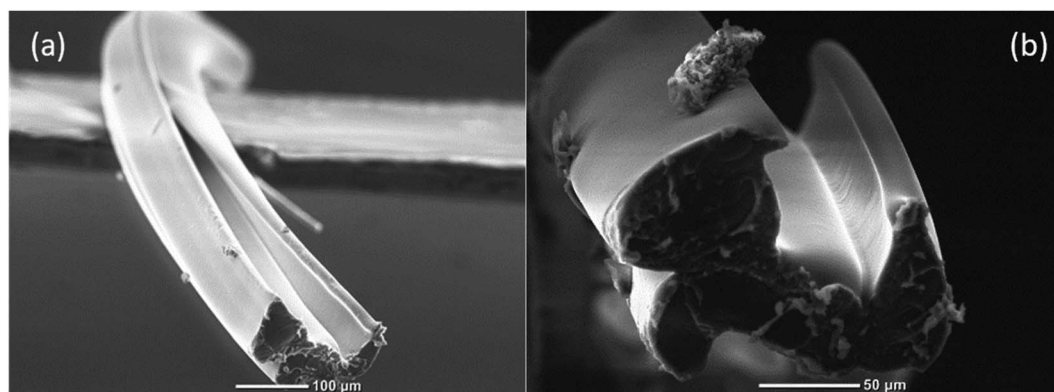

Fig. 5 (a) and (b) SEM images of the hollow microvessel fibers depicting the smoother surface topography of the inner walls.

the viscosities of the two aqueous solutions were similar, there was minimal resistance to the flow of one fluid by the other, and there was thus a negligible velocity gradient between them. Moreover, the higher the viscosities, the higher the resistance provided by the solutions to deformation due to shear force within the microfluidic device, thereby yielding smoother fibers as shown in Fig. 3. To examine the surface finish of the inner surface of the hollow microvessel fiber, a small perturbation was created in the water bath during the photopolymerization phase. Due to the disturbance in the water bath, the flow just leaving the microfluidic device was also disturbed and was solidified randomly upon application of UV light. This randomness in the flow allowed us to acquire images that clearly showed the inner surface finish of the hollow micro-vessel fiber (see Fig. 5). Since cells are in general greatly affected by their surrounding microenvironment, this additional control over the surface finish can provide some more predictability to the behavior of cells cultured in the hollow microvessel fibers. The biocompatibility and non-toxicity of PEGDA microfibers have already been shown by other groups.[33]

3. Conclusions

A micro-engineered device was created to develop biocompatible hollow microvessels having isotropic material characteristics and uniform inner dimensions throughout the length of the fiber. The goal of the project was to create hollow microvessel fibers that could mimic the characteristics of a microvasculature network comprised of arteries (0.1 mm to >1 cm), arterioles (10–100 μm), capillaries (4–12 μm), venules (10–100 μm), and veins (0.1 mm to >1 cm). Self-standing hollow microvessel fibers with inner dimensions as small as 15 μm to as large as 73 μm were fabricated. The comparatively large size of the chevrons provided enough space for the fluids to develop a uniform flow regime along and across the cross-section of the hollow microvessels, which resulted in the generation of smooth hollow fibers. The 50 wt% concentration of PEGDA575 in DI water provided the best balance of mechanical strength and cell non-toxicity.

Future work could include the alteration of the concentration of the PEGDA in the development of hollow microvessel fibers according to the degree of permeability required to mimic a specific physiological hollow microvessel. This work has established an important platform to successfully create hollow microvessel fibers that can be used to mimic a variety of microvasculature networks depending on the characteristics of the hollow microvessels.

4. Experimental

4.1. Materials

Poly(ethylene glycol) diacrylate (PEGDA, M_n = 400) and polyethylene glycol (PEG 400) were purchased from Aldrich Chemistry (St. Louis, MO). The photo-initiator Irgacure I2959 was purchased from BASF Dispersions & Pigments Asia Pacific. Deionized (DI) water was obtained by using a Thermo Fisher Scientific DI water system (Waltham, MA). Poly(methylmethacrylate) (PMMA)

(thickness of 6 mm) was purchased from Grainger. The prepolymer solution (cladding) was prepared by mixing PEGDA (50 wt%) and I2959 (4 wt%) with DI water and stirred until dissolved completely. Similarly, the core and the sheath solutions were prepared by mixing PEG (50 wt%) with DI water. A UV light source from Dymax Corporation (Torrington, CT) was used to photopolymerize the cladding solution. The intensity of the UV light used was 3.2 W cm^{-2} and this light was focused onto a 0.25 cm^2 area at the outlet of the microfluidic chip. Isopropyl alcohol was used as a rubbing reagent for PMMA chips prior to bonding to remove any dust particles from the chips. Ethyl alcohol (200 proof) was used as a reagent for bonding two PMMA chips in the presence of heat treatment.

A computerized numerical control (CNC) mini mill was purchased from Minitech Machinery Corporation (Norcross, GA). The poly(methyl methacrylate) (PMMA) chips were milled separately and bonded together to form a microfluidic device. AlTiN-coated end mill cutters and drill bits were purchased from Harvey tools and Grainger. The core channels were 1.00 mm × 0.75 mm (width × height). The chevrons for the first and second devices were 0.375 mm × 0.25 mm (width × height) and 0.381 mm × 0.381 mm (width × height), respectively.

4.2. Bonding methodology

After fabrication of both PMMA chips, they were precisely bonded together by using the solvent-assisted thermal bonding technique.[54] Bonding was the last step in this microfabrication and was one of the crucial steps in the process. The chips were first washed with ordinary detergent to remove simple fat and dust present on the surfaces of the chips. They were then rinsed with deionized water, and isopropyl alcohol was applied to the rinsed pieces. After the cleaning treatment with isopropyl alcohol, they were again rinsed with deionized water, and compressed air was used to blow dry them. Once the cleaning of the PMMA sheets was done, a fan-assisted oven was preheated to 74 °C. One of the PMMA sheets was covered with ethanol and the other PMMA sheet was placed on top of the first sheet. While overlaying the two PMMA sheets, it was made sure that the designs on both chips perfectly aligned together. After alignment of the chips, pressure was evenly applied with the help of two paper clamps on opposite ends of the chips, specifically on the longer sides. This assembly was then placed in a preheated oven for 10 minutes. After the heating process, the assembly was allowed to cool for 24 hours while applying a constant pressure to the clamps. Subsequently, the clamps were removed and a perfectly bonded PMMA chip was obtained as shown in the Fig. S1(a) (ESI†). A leakage test was performed by flowing dyed DI water through all of the inlets and the central channel. The dyed DI water was allowed to rest in the microchannel for an hour to check for any possible leakage spots. There was no evidence of dyed DI water in the areas except the milled channels as seen in Fig. S1(b) (ESI†).

4.3. Fabrication of hollow microvessels

For the production of hollow microvessels, the microfluidic device was held vertically above the DI water bath with the help

of paper clips and its tip slightly immersed in it. Separate syringes were filled with the core, cladding, and sheath solutions, and these solutions were then made to flow at specific flow rate ratios through their respective inlets using the syringe pumps as depicted in Fig. 4. The air pockets present in the microfluidic channel were removed by tapping the microfluidic device or flushing DI water through the outlet port of the device. Once the air pockets were removed from the microchannel, the fluids were allowed to flow until a stable flow regime was observed. A beam of UV light was then focused onto the microchannel at the lowest part of the microfluidic device. The microchannel along with chevrons were covered using aluminum foil to prevent the flow from subsequently clogging due to the UV light. Due to the photopolymerization reaction, the prepolymer solution (PEGDA) solidified to form hollow microvessels and the core and sheath solutions ran off into the DI water bath. The generated hollow microvessels were collected using a copper wire and were safely mounted on the paper frames. The fibers were allowed to sit overnight for drying at room temperature.

4.4. SEM imaging

Images of the hollow microfibers were captured by mounting the fibers on paper frames, which were eventually inserted into a JEOL JCM-6000 Benchtop SEM using carbon NEM tape (Nisshin EM. CO., LTD, Tokyo, Japan).

Conflicts of interest

The authors declare no conflict of interest.

Acknowledgements

References

1 S. G. Rayner and Y. Zheng, Engineered Microvessels for the Study of Human Disease, *J. Biomech. Eng.*, 2016, **138**(11), DOI: 10.1115/1.4034428.

2 M. G. Scioli, A. Bielli, G. Arcuri, A. Ferlosio and A. Orlandi, Ageing and microvasculature, *Vasc. Cell*, 2014, **6**, 1–19.

3 E. Okabe, K. Todoki and H. Ito, Microcirculation: function and regulation in microvasculature, in *Dynamic Aspects of Dental Pulp*, Springer, Dordrecht, 1990, pp. 151–166.

4 A. J. H. M. Houben, R. J. H. Martens and C. DA Stehouwer, Assessing microvascular function in humans from a chronic disease perspective, *J. Am. Soc. Nephrol.*, 2017, **28**(12), 3461–3472.

5 W. D. Tucker and K. Mahajan, Anatomy, blood vessels, in *StatPearls [Internet]*, StatPearls Publishing, 2018.

6 S. -W. SU, M. Catherall and S. Payne, The influence of network structure on the transport of blood in the human cerebral microvasculature, *Microcirculation*, 2012, **19**(2), 175–187.

7 M. G. Musa, C. Torrens and G. F. Clough, The microvasculature: a target for nutritional programming and later risk of cardio-metabolic disease, *Acta Physiol.*, 2014, **210**(1), 31–45.

8 F. Feihl, L. Liaudet, W. Bernard and B. I. Levy, Hypertension: a disease of the microcirculation?, *Hypertension*, 2006, **48**(6), 1012–1017.

9 D. D. Gutterman, D. S. Chabowski, A. O. Kadlec, M. J. Durand, J. K. Freed, K. Ait-Aissa and A. M. Beyer, The human microcirculation: regulation of flow and beyond, *Circ. Res.*, 2016, **118**(1), 157–172.

10 R. R. S. Costa, N. Ribeiro Villela, C. Souza Maria das Graças, B. C. S. Boa, F. Z. G. A. Cyrino, S. V. Silva, P. C. Lisboa, E. G. Moura, T. C. Barja-Fidalgo and E. Bouskela, High fat diet induces central obesity, insulin resistance and microvascular dysfunction in hamsters, *Microvasc. Res.*, 2011, **82**(3), 416–422.

11 A. Corstian, E. Klijn, W. K. Lagrand, J. J. Brugts, C. Ince, P. E. Spronk and M. L. Simoons, The microcirculation in health and critical disease, *Prog. Cardiovasc. Dis.*, 2008, **51**(2), 161–170.

12 C. Ince, The microcirculation is the motor of sepsis, *Crit. Care*, 2005, **9**(4), S13.

13 P. E. Spronk, D. F. Zandstra and C. Ince, Bench-to-bedside review: sepsis is a disease of the microcirculation, *Crit. Care*, 2004, **8**(6), 462.

14 D. V. Horbelt, D. K. Roberts, T. H. Parmley and N. J. Walker, Ultrastructure of the microvasculature in human endometrial hyperplasia, *Am. J. Obstet. Gynecol.*, 1996, **174**(1), 174–183.

15 M. A. Khan, F. Alanazi, H. A. Ahmed, F. H. Al-Mohanna, A. M. Assiri and D. Clemens Broering, FOXP3$^+$ regulatory T cell ameliorates microvasculature in the rejection of mouse orthotopic tracheal transplants, *J. Clin. Immunol.*, 2017, **174**, 84–98.

16 M. P. McInerney, Y. Pan, I. Volitakis, A. I. Bush, J. L. Short and J. A. Nicolazzo, The Effects of Clioquinol on P-glycoprotein Expression and Biometal Distribution in the Mouse Brain Microvasculature, *J. Pharm. Sci.*, 2019.

17 W. Lu, Z. Dong, Z. Liu, W. Fu, Y. Peng, S. Chen, T. Xiao, *et al.*, Detection of microvasculature in rat hind limb using synchrotron radiation, *J. Surg. Res.*, 2010, **164**(1), e193–e199.

18 M. Sato and N. Ohshima, Hemodynamics at stenoses formed by growing platelet thrombi in mesenteric microvasculature of rat, *Microvasc. Res.*, 1986, **31**(1), 66–76.

19 J. O. R. G. E. Boczkowski, E. R. I. C. Vicaut and M. I. C. H. E. L. Aubier, In vivo effects of Escherichia coli endotoxemia on diaphragmatic microcirculation in rats, *J. Appl. Physiol.*, 1992, **72**(6), 2219–2224.

20 J. Fox, G. Frank and H. Wayland, Action of histamine on the mesenteric microvasculature, *Microvasc. Res.*, 1980, **19**(1), 108–126.

21 B. R. Johansson, Size and distribution of endothelial plasmalemmal vesicles in consecutive segments of the

microvasculature in cat skeletal muscle, *Microvasc. Res.*, 1979, **17**(2), 107–117.

22 A. G. Harris, I. Sinitsina and K. Messmer., Validation of OPS imaging for microvascular measurements during isovolumic hemodilution and low hematocrits, *Am. J. Physiol.: Heart Circ. Physiol.*, 2002, **282**(4), H1502–H1509.

23 R. R. S. Costa, N. Ribeiro Villela, C. Souza Maria das Graças, B. C. S. Boa, F. Z. G. A. Cyrino, S. V. Silva, P. C. Lisboa, E. G. Moura, T. C. Barja-Fidalgo and E. Bouskela, High fat diet induces central obesity, insulin resistance and microvascular dysfunction in hamsters, *Microvasc. Res.*, 2011, **82**(3), 416–422.

24 F. M. Vega, V. Gautier, C. M. Fernandez-Ponce, M. J. Extremera, A. F. M. Altelaar, J. Millan, J. C. Tellez, *et al.*, The atheroma plaque secretome stimulates the mobilization of endothelial progenitor cells ex vivo, *J. Mol. Cell. Cardiol.*, 2017, **105**, 12–23.

25 N. S. Kleiman, N. Grazeiadei, M. Kelly, R. J. Taylor, B. Frederick, E. T. Lance, M. B. Effron, R. E. Jordan and M. A. Mascelli, Abciximab, ticlopidine, and concomitant abciximab-ticlopidine therapy: ex vivo platelet aggregation inhibition profiles in patients undergoing percutaneous coronary interventions, *Am. Heart J.*, 2000, **140**(3), 492–501.

26 R. L. Pemathilaka, J. D. Caplin, S. S. Aykar, R. Montazami and N. N. Hashemi, Placenta-on-a-Chip: In Vitro Study of Caffeine Transport across Placental Barrier Using Liquid Chromatography Mass Spectrometry, *Global Challenges*, 2019, **3**(3), 1800112.

27 R. L. Pemathilaka, D. E. Reynolds and N. N. Hashemi, Drug transport across the human placenta: review of placenta-on-a-chip and previous approaches, *Interface focus*, 2019, **9**(5), 20190031.

28 K. H. K. Wong, J. M. Chan, R. D. Kamm and J. Tien, Microfluidic models of vascular functions, *Annu. Rev. Biomed. Eng.*, 2012, **14**, 205–230.

29 J. D. Caplin, N. G. Granados, M. R. James, R. Montazami and N. Hashemi., Microfluidic organ-on-a-chip technology for advancement of drug development and toxicology, *Adv. Healthcare Mater.*, 2015, **4**(10), 1426–1450.

30 Z. Bai, M. Janet, M. Reyes, R. Montazami and N. Hashemi, On-chip development of hydrogel microfibers from round to square/ribbon shape, *J. Mater. Chem. A*, 2014, **2**(14), 4878–4884.

31 N. Hashemi, J. M. Lackore, F. Sharifi, P. J. Goodrich, M. L. Winchell and N. Hashemi., A paper-based microbial fuel cell operating under continuous flow condition, *Technology*, 2016, **4**(02), 98–103.

32 H. Acar, S. Çınar, M. Thunga, M. R. Kessler, N. Hashemi and R. Montazami, Study of physically transient insulating materials as a potential platform for transient electronics and bioelectronics, *Adv. Funct. Mater.*, 2014, **24**(26), 4135–4143.

33 F. Sharifi, B. B. Patel, M. C. McNamara, P. J. Meis, M. N. Roghair, M. Lu, R. Montazami, D. S. Sakaguchi and N. N. Hashemi, Photo-cross-Linked Poly(ethylene glycol) Diacrylate Hydrogels: Spherical Microparticles to Bow Tie-shaped Microfibers, *ACS Appl. Mater. Interfaces*, 2019.

34 F. Sharifi, B. B. Patel, A. K. Dzuilko, R. Montazami, D. S. Sakaguchi and N. Hashemi, Polycaprolactone microfibrous scaffolds to navigate neural stem cells, *Biomacromolecules*, 2016, **17**(10), 3287–3297.

35 D. Sechi, B. Greer, J. Johnson and N. Hashemi, Three-dimensional paper-based microfluidic device for assays of protein and glucose in urine, *Anal. Chem.*, 2013, **85**(22), 10733–10737.

36 R. G. Bardón, A. Passos, M. Piergiovanni, S. Balabani, G. Pennati and G. Dubini, Haematocrit heterogeneity in blood flows past microfluidic models of oxygenating fibre bundles, *Med. Eng. Phys.*, 2019.

37 T. H. Petersen, E. A. Calle, L. Zhao, E. J. Lee, L. Gui, M. B. Raredon, K. Gavrilov, *et al.*, Tissue-engineered lungs for in vivo implantation, *Science*, 2010, **329**(5991), 538–541.

38 H. C. Ott, T. S. Matthiesen, S.-K. Goh, L. D. Black, S. M. Kren, T. I. Netoff and D. A. Taylor, Perfusion-decellularized matrix: using nature's platform to engineer a bioartificial heart, *Nat. Med.*, 2008, **14**(2), 213.

39 A. J. Milici, M. B. Furie and W. W. Carley, The formation of fenestrations and channels by capillary endothelium in vitro, *Proc. Natl. Acad. Sci. U. S. A.*, 1985, **82**(18), 6181–6185.

40 H. Uwamori, Y. Ono, T. Yamashita, K. Arai and R. Sudo, Comparison of organ-specific endothelial cells in terms of microvascular formation and endothelial barrier functions, *Microvasc. Res.*, 2019, **122**, 60–70.

41 V. M. Dominical, D. M. Vital, F. O. '. Dowd, S. T. O. Saad, F. F. Costa and N. Conran, In vitro microfluidic model for the study of vaso-occlusive processes, *Exp. Hematol.*, 2015, **43**(3), 223–228.

42 M. Tsai, A. Kita, J. Leach, R. Ross, J. N. Huang, J. Moake, R. E. Ware, D. A. Fletcher and W. A. Lam, In vitro modeling of the microvascular occlusion and thrombosis that occur in hematologic diseases using microfluidic technology, *J. Clin. Invest.*, 2011, **122**(1).

43 M. A. Daniele, K. Radom, F. S. Ligler and A. A. Adams, Microfluidic fabrication of multiaxial microvessels via hydrodynamic shaping, *RSC Adv.*, 2014, **4**(45), 23440–23446.

44 Ke Luo, N. Yudewitz, G. Subhash and D. E. Spearot, Effect of water concentration on the shock response of polyethylene glycol diacrylate (PEGDA) hydrogels: a molecular dynamics study, *J. Mech. Behav. Biomed. Mater.*, 2019, **90**, 30–39.

45 T. Eshel-Green, S. Eliyahu, S. Avidan-Shlomovich and H. Bianco-Peled, PEGDA hydrogels as a replacement for animal tissues in mucoadhesion testing, *Int. J. Pharm.*, 2016, **506**(1–2), 25–34.

46 D. Debroy, J. Oakey and D. Li, Interfacially-mediated oxygen inhibition for precise and continuous poly(ethylene glycol) diacrylate (PEGDA) particle fabrication, *J. Colloid Interface Sci.*, 2018, **510**, 334–344.

47 B. Xia, Z. Jiang, D. Debroy, D. Li and J. Oakey, Cytocompatible cell encapsulation via hydrogel photopolymerization in microfluidic emulsion droplets, *Biomicrofluidics*, 2017, **11**(4), 044102.

48 A. K. Price and C. T. Culbertson, Generation of nonbiased hydrodynamic injections on microfluidic devices using

integrated dielectric elastomer actuators, *Anal. Chem.*, 2009, **81**(21), 8942–8948.

49 J. Jeon, N. Choi, H. Chen, J.-Il Moon, L. Chen and J. Choo, SERS-based droplet microfluidics for high-throughput gradient analysis, *Lab Chip*, 2019, **19**(4), 674–681.

50 W. Je. Jeong, J. Y. Kim, J. Choo, E. K. Lee, C. S. Han, D. J. Beebe, H. S. Gi and S. H. Lee, Continuous fabrication of biocatalyst immobilized microparticles using photopolymerization and immiscible liquids in microfluidic systems, *Langmuir*, 2005, **21**(9), 3738–3741.

51 R. Al Nuumani, G. Bolognesi and G. T. Vladisavljevic, Microfluidic production of poly (1,6-hexanediol diacrylate)-based polymer microspheres and bifunctional microcapsules with embedded TiO$_2$ nanoparticles, *Langmuir*, 2018, **34**(39), 11822–11831.

52 R. Knob, R. L. Hanson, O. B. Tateoka, R. L. Wood, I. Guerrero-Arguero, R. A. Robison, W. G. Pitt and A. T. Woolley, Sequence-specific sepsis-related DNA capture and fluorescent labeling in monoliths prepared by single-step photopolymerization in microfluidic devices, *J. Chromatogr. A*, 2018, **1562**, 12–18.

53 Z. Jiang, B. Xia, R. McBride and J. Oakey, A microfluidic-based cell encapsulation platform to achieve high long-term cell viability in photopolymerized PEGNB hydrogel microspheres, *J. Mater. Chem. B*, 2017, **5**(1), 173–180.

54 A. Bamshad, A. Nikfarjam and H. Khaleghi, A new simple and fast thermally-solvent assisted method to bond PMMA–PMMA in micro-fluidics devices, *J. Micromech. Microeng.*, 2016, **26**(6), 065017.